

Development of Novel Nsp16 Inhibitors as Potential Anti-SARS-CoV-2 Agents

*Kuojun Zhang*¹, *Alexey V. Sulimov*², *Ivan S. Ilin*², *Danil C. Kutov*²,
*Anna S. Taschilova*², *Sheng Jiang*¹, *Tianyu Wang*¹, *Vladimir B. Sulimov*²,
*Yibei Xiao*¹

© The Authors 2024. This paper is published with open access at SuperFri.org

Computer aided structural based approach was used to find inhibitors of SARS-CoV-2 nsp16 (2'-O-methyltransferase). Docking based virtual screening of three libraries, Enamine Coronavirus Library, Enamine Nucleoside Mimetics Library, and Chemdiv Nucleoside Analogue Library, was performed. In total, 39350 3D-structures of low molecular weight ligands were docked into a model of nsp16 prepared using the structure of 6WKQ complex from the Protein Data Bank. Docking was performed by the SOL docking program. For the best SOL scored ligands, the protein-ligand binding enthalpy was calculated using the PM7 semiempirical quantum-chemical method with the COSMO implicit solvent model. The most promising eleven compounds were purchased and their inhibitory activity against the recombinant viral nsp16 protein was measured using MST assay with Monolith NT.115. As a result, two compounds, Z195979162 and Z1333277068, from Enamine Coronavirus Library demonstrated dissociation constants K_d for nsp16/nsp10 complex equal to 2.0 and 5.0 μM . The relative stability of these ligands in their docked positions in the nsp16 S-adenosylmethionine (SAM) binding site was confirmed in the molecular dynamics simulations along 70 ns trajectories. Z195979162 and Z1333277068 compounds belong to two chemical classes: 1,4-disubstituted tetrahydropyridines and derivatives of pyrazole-5-carboxamide, respectively, and can be good starting points for further hit optimization in the field of nsp16 inhibitors design.

Keywords: nsp16, methyltransferase, virtual screening, protein-ligand binding, enzyme inhibitors, recombinant protein expression, SARS-CoV-2.

Introduction

The 2019 coronavirus disease (COVID-19) pandemic caused by the severe acute respiratory syndrome coronavirus 2 (SARS-CoV-2) still poses a great threat to the global public health. According to the WHO report, there have been 632 million confirmed cases and more than 6.5 million deaths worldwide, as of November 2022. SARS-CoV-2 is evolving and new infectious and antibody-resistant strains are emerging [17]. Although highly effective SARS-CoV-2 vaccines have been used globally, increasing number of breakthrough infections have been observed in fully vaccinated individuals, mainly due to compromised effectiveness against the emerging variants, such as Delta and Omicron [15, 28]. Nirmatrelvir, an inhibitor of SARS-CoV-2 main protease, which was granted FDA Emergency Use Authorization at the end of 2021 and discovered rationally, not by re-purposing of existing drugs represents the only direct-acting agent of such type in scarce arsenal of anti-coronavirus treatment [11, 32]. The public are hence still at high risk of being infected, and consequently the need for innovative and effective antivirals against SARS-CoV-2 and the emerging variants is still highly needed and unmet.

The fight against this disease includes various tasks, including the development of direct-acting antiviral drugs on therapeutic target proteins of the SARS-CoV-2 coronavirus. By the beginning of the pandemic, information about the mechanisms of coronavirus replication already existed thanks to research on SARS-CoV and MERS-CoV coronaviruses, which caused two major outbreaks of deadly pneumonia in 2002 and 2012, respectively [50, 51].

¹School of Pharmacy, China Pharmaceutical University, Nanjing, China

²Research Computer Center of Lomonosov Moscow State University, Moscow, Russian Federation

SARS-CoV-2's genome codes 29 proteins, several of which have been exploited as potential therapeutic targets for the development of new antivirals [18, 39, 46, 52, 53]. In this work, we chose nonstructural protein 16 (nsp16), the viral RNA 2'-O-Methyltransferase (2'-O-MTase) [45]. Nsp16 has been considered as an attractive target for antiviral therapeutics due to its key role in the formation of a viral RNA cap. Specially, nsp16 and nsp10 form a heterodimer and function to catalyze the transfer of a methyl group from its co-substrate S-adenosylmethionine (SAM, **1**) in Fig. 1 to the first transcribed nucleotide at the 2'-OH position, converting the cap-0 structure (featured as 7MeGpppA...) into the cap-1 structure (featured as 7MeGpppA2'-O-Me...) [13]. 2'-O-methylation is necessary for the formation of the cap structure in viral RNAs, which makes it possible to read the SARS-CoV-2 genetic information by the host translation mechanism. This 2'-O-MTase has been shown to be indispensable for the replication of coronaviruses in cell cultures [16, 25, 34, 35]. This methylation process plays an important role in the translation of viral proteins, protection of the nascent viral mRNA from exonucleases, and evasion of host immunity [10, 29]. SAM contains an activated methyl group and is a common co-substrate for methyl transfer reactions in living organisms. Thus, blocking the SAM binding site of nsp16 leads to inhibition of the methylation process catalyzed by this enzyme. Moreover, 2'-O-MTase/nsp16 is highly conserved among various coronavirus species, also making it a potential effective target for the development of broad-spectrum antivirals [10]. Furthermore, crystal structures of SARS-CoV-2 nsp16/nsp10 complex alone and in complex with RNA, SAM, or SAM analogs have been reported [24, 25, 27, 37, 48], which provides structural basis for structure-based inhibitor design and virtual screening approaches.

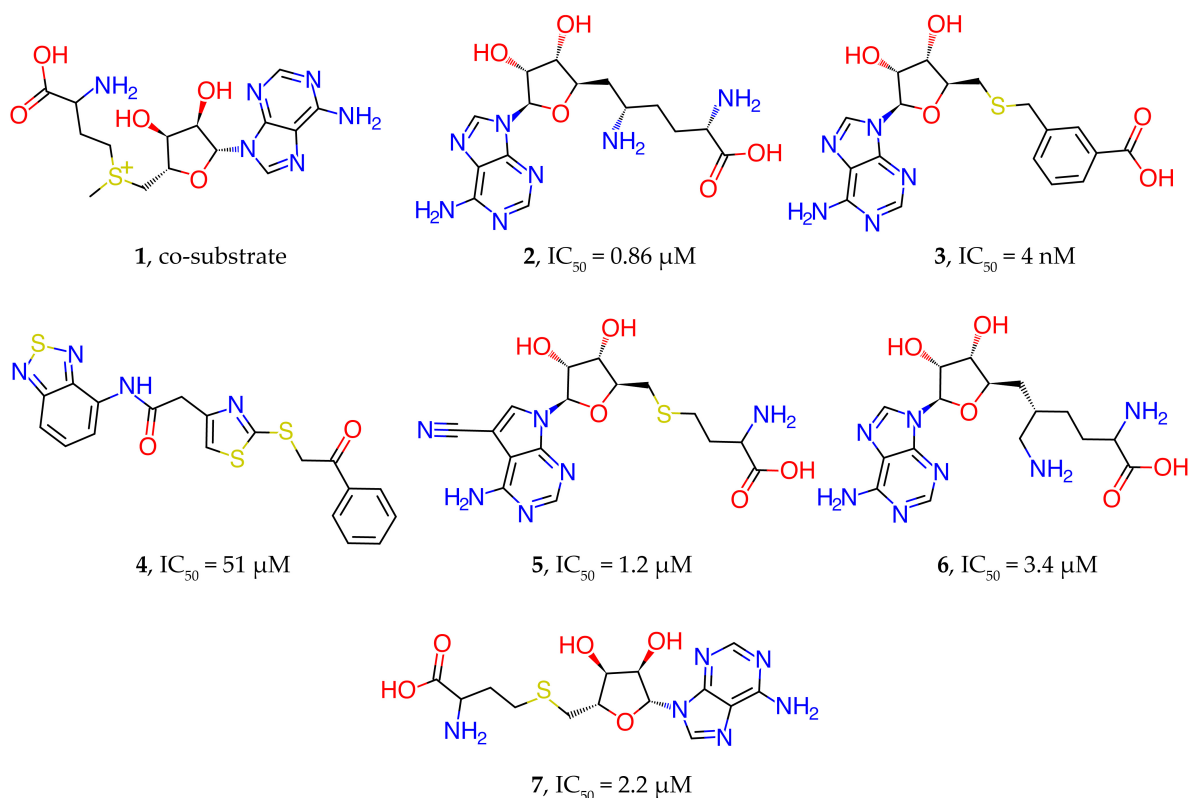


Figure 1. Experimentally confirmed nsp16 inhibitors

Nsp16 was studied during the outbreak of SARS-CoV pneumonia, which led to the identification of a strong suppressor of nsp16 methyltransferase activity, sinefungin **2** in Fig. 1 [12]. Sinefungin, like SAM, an endogenous cofactor of nsp16, binds in the same pocket. The activity of sinefungin against SARS-CoV-2 nsp16 was also confirmed by X-ray diffraction analysis [25]. Sinefungin was reported to be a potent 2'-O-MTase inhibitor against vaccinia virus, MERS-CoV, SARS-CoV and SARS-CoV-2. Recently, Bobileva et al. reported a series of sinefungin derivatives, exemplified by compound **3** (Fig. 1), by using bioisosteric substitution of the sulfonium and amino acid substructures aided by docking model [8]. Compound **3** exhibited high inhibitory potency against SARS-CoV-2 nsp16 and nsp14 with IC₅₀ values 4.0 and 8.0 nM, respectively. However, it is nonselective against human glycine N-methyltransferase (GNMT) (IC₅₀ = 8.6 nM). The main reason for the non-selectivity may be related to the very high similarity between the nsp16 inhibitors found and S-adenosylmethionine, the cofactor used by most methyltransferases.

Employing a high throughput virtual screening (vHTS) based on the docking of 7 million commercially available drug compounds and SAM analogues, Bobrovs et al. identified some inhibitors against nsp14 and nsp16 [9]. Among them, the best compound ZINC38661771 **4** (Fig. 1) with a sulfanylthiazole core exhibited inhibitory activity against nsp14 and nsp16 with IC₅₀ values of 118 and 51 μ M, respectively, but this compound was also active against GNMT with IC₅₀ value of 58 μ M.

Through cross-screening of SARS-CoV-2 nsp14 inhibitors against nsp10/nsp16 complex, Klima et al. identified two nsp16 inhibitors SS148 **5** and WZ16 **6** (Fig. 1) with IC₅₀ = 1.2 and 3.4 μ M, respectively [24]. The IC₅₀ value determined for S-adenosylhomocysteine (SAH) **7** (Fig. 1) used as a control was 2.2 ± 0.2 μ M. Also, in this work, the crystal structures of nsp10/nsp16 complex with the found inhibitors SS148 (PDB ID: 7R1T) and WZ16 (PDB ID: 7R1U) were presented.

At the moment, there are many studies using various computer modeling methods such as molecular docking, molecular dynamics, quantum chemical calculations, machine learning methods to identify nsp16 inhibitors. However, most of these studies do not include experimental validation of the inhibitory activity of the candidates found.

A large-scale study on the identification of nsp16 inhibitors was carried out in [14]. A 3D pharmacophore model based on the nsp16-sinefungin complex (PDB ID: 6WKQ) screened 48 million drug-like compounds from the ZINC database. The 24 best performing molecules were placed in the SAM binding pocket. Molecular dynamics simulations were performed for the top three compounds, and one compound **8** (see Fig. 2) with a triazine backbone was identified as a potential inhibitor of nsp16.

In a study [38], several inhibitors of nsp16 were identified by computer simulations, without confirmation of *in vitro* activity. Pharmacophore screening of the Bionet and Chemdiv databases was carried out, followed by molecular docking into the nsp16 active pocket by Glide, molecular dynamics simulations and binding free energy calculations. Based on results of virtual screening two compounds **9** and **10** were sorted out as potential nsp16 inhibitors (Fig. 2). These compounds can form a stable complex with the protein and form strong hydrogen bonds and salt bridges with the key amino acids Asp6897 and Asp6928.

Mohammad et al. discovered genquanin-6-C-beta-glucopyranoside (**11**, Fig. 2) as a potential nsp16 inhibitor via screening the North African Natural Products database for compounds that can interact with the nsp10 interface and disrupt the formation of the nsp10/nsp16 complex [30].

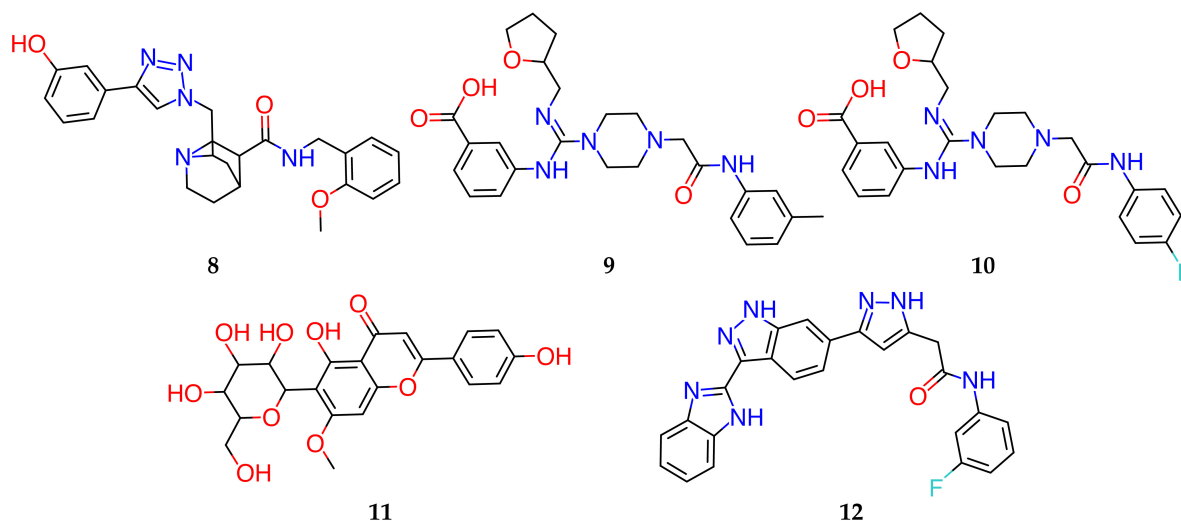


Figure 2. Inhibitors of the 2'-O-MTase activity of nsp10/nsp16 complex, predicted by molecular modeling in the literature, which have not yet received experimental confirmation of their inhibitory activity

The best binding affinity was predicted for four compounds using AutoDock Vina. Further, molecular dynamics simulations were performed for these four compounds and genquanin-6-C-beta-glucopyranoside showed the most stable complex with nsp10, but was not tested *in vitro*.

A search for inhibitors of 2'-O-MTase activity of the nsp10/nsp16 complex in the PubChem and anti-HIV databases was carried out using a multi-stage virtual screening protocol, including Lipinski's rule filtering, docking, and steered molecular dynamics [31]. As a result, the best candidate CID 135566620 (**12**, Fig. 2) from PubChem was predicted to possess inhibition constant in the submicromolar range. *In vitro* and *in vivo* testing to confirm the activity of this nsp10/nsp16 inhibitor candidate has not been performed. A virtual molecular docking was carried out to screen inhibitors against nsp10/nsp16 2'-O-MTase activity from a library of compounds that were found in the ZINC database, in plants of the Caatinga Brazilian biome, as well as structural analogues of SAM and sinefungin (SFG) at PubChem database [19]. Docking was performed using AutoDock Vina, and 24 potential 2'-O-MTase inhibitors were identified in all the studied sets of molecules, among which the most promising were 5 compounds from the ZINC database.

In this work, a virtual screening of chemical compounds from three libraries using docking was carried out, followed by a quantum-chemical calculation of the enthalpy of binding of a ligand to the protein in order to search for nsp16 inhibitors. The SAM-binding site of the enzyme was used as a target to inhibit the 2'-O-MTase activity. As a result, eleven compounds were selected for experimental validation of their binding to nsp16; for two of them, belonging to two chemical classes, 1,4-disubstituted tetrahydropyridines and derivatives of pyrazole-5-carboxamide, the binding affinity with K_d of 2.0 and 5.0 μM was experimentally confirmed. Molecular dynamics studies additionally confirmed stability of complexes of these two compounds with nsp16.

The article is organized as follows. Section 1 describes the modeling methods used in virtual screening, the study of the stability of inhibitors in docked positions using molecular dynamics, and experimental techniques for measuring the inhibitory activity of selected compounds. In section 2 we present results of our study. Conclusion summarizes the study and points directions for further work.

1. Materials and Methods

1.1. Virtual Screening

Virtual screening of three chemical libraries was performed using the SOL docking program [43, 44]. These libraries were: Enamine Coronavirus Library, Enamine Nucleoside Mimetics Library, and Chemdiv Nucleoside Analogue Library. Enamine libraries were downloaded in SDF format from here [2]. Chemdiv Nucleoside Analogue Library also in SDF format was downloaded from here [1]. Prior to ligand preparation, we filtered out PAINS (Pan Assay Interference Compounds) [6] molecules from all three libraries. The LigPrep tool [5] was applied to protonate ligands from these libraries and generate three-dimensional conformers for each ligand. In case of Enamine Coronavirus Library, from initial 16800 compounds 16561 organic molecules were left after PAINS filtering and 34405 unique 3D conformers were generated by LigPrep. For Enamine Nucleoside Mimetics Library, 276 of 290 compounds were retained during PAINS filtering which were converted into 898 conformers by LigPrep. For the third library, Chemdiv Nucleoside Analogue Library, PAINS filtering retained 2107 of 2600 initial compounds and 4047 conformers were generated for them. To sum up, 39350 unique 3D molecules were virtually screened against nsp16 in the frame of the study.

A model of the nsp16 protein was prepared using the protein structure from the 6WKQ crystal complex [37] stored in the Protein Data Bank (PDB) [7]. This complex consisted of the SARS-CoV-2 nsp16/nsp10 heterodimer with sinefungin crystallized in a SAM-binding site of nsp16 and possessed excellent resolution (1.98 Å) with only four missed residues on N-terminus. These residues were not repaired in our model due to their distant position from the site selected for docking. The protein model was prepared by removing the nsp10 part of the heterodimer and adding hydrogen atoms using the Aplate program [26], which protonates protein atoms at pH 7.4. A grid of potentials was constructed by the SOLGRID module [43, 44]. The model was validated by docking known nsp16 inhibitors using the SOL program [43, 44]: sinefungin in a co-crystallized and partially neutralized form and S-Adenosyl-L-homocysteine extracted from another PDB complex, 6WJT. Positioning of sinefungin (in a partially neutralized form) resulted in the scoring-function of -7.07 kcal/mol and the reproduction of a crystalized pose (RMSD = 0.87 Å). Docking of S-Adenosyl-L-homocysteine gave scoring-function of -7.48 kcal/mol and the similar conformation observed in the complex of nsp16 with S-Adenosyl-L-homocysteine: RMSD between a docked pose and a quasi-native conformation obtained from alignment of 6WJT on 6WKQ was 0.97 Å. Details of the protein model preparation and validation are presented in [42].

The SOL docking program performed grid-based docking utilizing genetic algorithm for conformational sampling and physics-based scoring-function which contained interactions terms from the MMFF94 force field [21] and a desolvation term based on a simplified form of the Generalized Born solvation model [36]. The flexibility of a ligand was encoded by translation and rotation of a ligand as a rigid body and rotations of each rotatable bond. Since conformations of macrocycles were not sampled, they were generated preliminary for each ligand with such cycles at the stage of library preparation. The conformation of the protein was fixed during docking. Genetic algorithm used for a global optimization task was applied with the following parameters: population size was 30000, the number of generations was 1000, and the number of independent runs was 50. Independent runs helped to assess how well the conformational space of a given ligand was explored by docking. In other words, it gave one an opportunity to assess reliability of the found global energy minimum: if independent runs converged well and many of them resulted

in the same best solution, it increased certainty in the identified best docking pose. Technically, such convergence was estimated by cluster analysis. If RMSD between two poses was less than 1 Å, they were included in one cluster. Convergence was expressed in a small number of clusters and a high population for the first cluster, which contained the docked pose of the ligand with the lowest energy – the best docked pose. In each run, the best ligand docked pose corresponded to the most negative value of the objective function of the global optimization employed by the SOL docking algorithm. The objective function was the sum of the ligand energy in the protein field and the internal strain energy of the ligand calculated in the MMFF94 force field. To accelerate the virtual screening of libraries with thousands of compounds, this study used SOL installed on the Lomonosov-2 supercomputer [49] of Lomonosov Moscow State University with docking of each ligand on a separate computing core.

In order to evaluate the affinity of ligands for nsp16 better, the protein-ligand binding enthalpy ΔH_{bind} was calculated by MOPAC [4] using the PM7 quantum-chemical semiempirical method [40] for top scored ligands predicted by docking. The binding enthalpy was obtained by calculating three terms: the enthalpy of formation of a protein-ligand complex, the enthalpy of formation of an unbound ligand, and the enthalpy of formation of an unbound protein molecule. The first term was calculated in two stages including optimization of the PM7 energy of the protein-ligand complex by varying Cartesian coordinates of all ligand atoms from the initial geometry predicted by docking followed by calculation of enthalpy of formation of the protein-ligand complex for the optimized geometry using the PM7 method with the COSMO implicit solvation model [23]. To handle calculation for such big molecular system as a protein-ligand complex, MOZYME module [41] was applied. The similar procedure was performed for calculation of the enthalpy of formation of an unbound ligand. The enthalpy of formation of unbound protein was calculated for the fixed conformation used during docking. The final value of ΔH_{bind} was found according to the following equation:

$$\Delta H_{bind} = \Delta H_{complex} - \Delta H_{protein} - \Delta H_{ligand}, \quad (1)$$

$\Delta H_{complex}$ is the enthalpy of formation of the protein-ligand complex, $\Delta H_{protein}$ is the enthalpy of formation of an unbound protein, ΔH_{ligand} is the enthalpy of formation of an unbound ligand.

The final prioritization of compounds for purchasing and testing was performed with considering three criteria: the most negative values of the SOL scoring function and ΔH_{bind} , and geometric features of the ligand pose after optimization in PM7. The latter implies visual estimation of ligand complementarity to an active site of nsp16, ligand distortion and presence of key interactions between nsp16 and the ligand.

1.2. Molecular Dynamics Simulation

To illustrate stability of the nsp10/nsp16 complex with our two inhibitors, we performed a molecular dynamics (MD) simulation of the system along a relatively long trajectory of several dozen ns. Besides these two molecules, sinefungin and C692-0494 were simulated to obtain, respectively, positive and negative control. We used the NAMD [33] package (<http://www.ks.uiuc.edu/Training/Tutorials/namd>), the CHARMM36 all-atom additive force field, and NPT ensemble, when the number of the particle N, pressure P, and temperature T were constants. Initial poses were taken from docking studies.

Nsp16 protein preparation included specification of exact protonation state for histidine residues with replacing generic HIS notation with one of three options: HSD (neutral side group, proton on the ND1 atom), HSE (neutral side group, proton on the NE2 atom), HSP (charged histidine, proton on both ND1 and NE2). These states were determined manually via observation of the protein structure after protonation. Preparation of the PSF files was performed by VMD [3].

Ligands were parametrized in CHARMM general force field [47] using web tool: <https://cgenff.umaryland.edu/>. To facilitate trajectory analysis, the protein-ligand complex was moved to the origin. Solvation was carried out in VMDs solvated plugin with constructing $60 \times 60 \times 60 \text{ \AA}$ box with TIP3P water molecules and applying 8 \AA padding. The specified 8 \AA padding creates the water box sized such that in each direction from the atom with the largest coordinate in that direction there is an 8 \AA layer of water to provide enough space for the mobility of the protein-ligand complex. The autoionize plugin of VMD was applied to neutralize the system by addition of counterions. In total, each prepared system included about 40000 atoms with about 11500 water molecules. For complex nsp16 with C692-0494, two different solvation models were used: TIP3P and SPC.

The molecular dynamic simulation for each complex consisted of three steps: minimization, equilibration and production run. Firstly, minimization was performed for each complex and consisted of 5000 steps. After that, 1 ns of equilibration was followed by a 72 ns unrestrained production run at 310 K and 1 atm. Langevin dynamics was used for constant temperature control and constant pressure control. Periodic boundary conditions were applied and the time step of the MD trajectory was 1 fs. For all calculations resources of the Lomonosov-2 supercomputer [49] of Lomonosov Moscow State University were used. Calculation of equilibration step (1 ns) took about 70 minutes using 32 cores. To calculate full production run (72 ns), it took about 2800 minutes using 64 cores for each complex.

To analyse trajectories, the MDAnalysis library was applied [20]. A plot of RMSD change over time was prepared using the Matplotlib library [22]. RMSD is the root-mean square deviation of the corresponding ligand from its docked position in the enzyme.

1.3. Protein Production and Purification

The co-expressed nsp16 and nsp10 proteins were cloned into modified pETduet-1 vector, with N terminus possessing 6X His-tag in nsp10 while nsp16 bond to nsp10 without extra affinity tags. Briefly, *E. coli* BL21 (DE3) cells were transformed with the expression vector and grown at $37 \text{ }^\circ\text{C}$ in LB medium. After OD600 reached 0.6, the protein expression was induced by addition of IPTG to final concentration $500 \text{ }\mu\text{M}$ and the protein was expressed overnight at $18 \text{ }^\circ\text{C}$. The cells were harvested and the pellets were resuspended in a buffer (20 mM HEPES pH 8.0, 500 mM NaCl, 5 mM MgCl_2 , 10% glycerol) and homogenized with an ultrahigh-pressure cell disrupter at $4 \text{ }^\circ\text{C}$. The insoluble material was removed by centrifugation at 17000 rpm for 40 min. The protein complex was first purified by Ni-NTA affinity chromatography by wash buffer (20 mM HEPES pH 8.0, 500 mM NaCl, 5 mM MgCl_2 , 20 mM imidazole), then eluted by elution buffer (20 mM HEPES pH 8.0, 500 mM NaCl, 5 mM MgCl_2 , 300 mM imidazole). The proteins were purified by Superdex 10/300 columns. The nsp10/nsp16 complex was eluted as a single homogenous species in a final buffer containing 20 mM HEPES pH 8.0, 150 mM NaCl, 5 mM MgCl_2 .

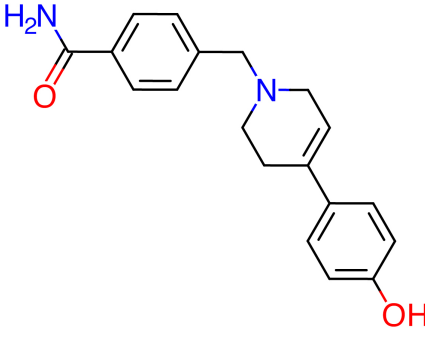
1.4. Determining Affinity of Compounds for Nsp16/Nsp10

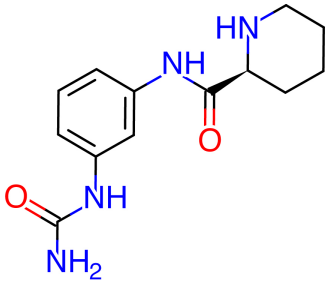
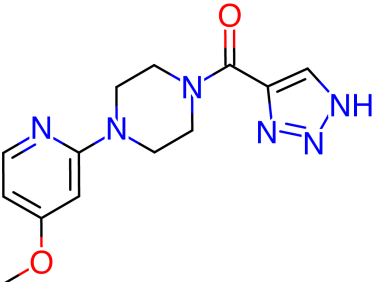
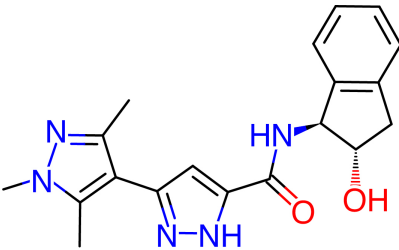
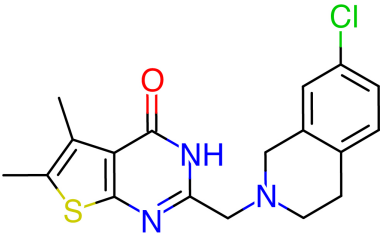
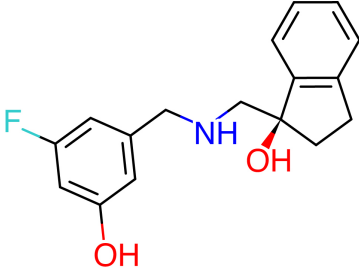
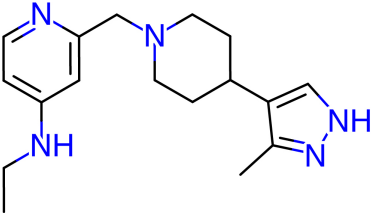
The purified nsp16/nsp10 protein complex was labeled with a protein labeling Kit (Monolith, RED-NHS 2nd Generation kit, Cat# MO-L011). In brief, 10 μM of protein was incubated with dye solution (30 μM) in the labeling buffer and the reaction was allowed to proceed at room temperature for 30 min. Each compound was dissolved in the Microscale thermophoresis (MST) reaction buffer containing 20 mM HEPES pH 8.0, 150 mM NaCl, 5 mM MgCl_2 . Two-fold serial dilutions started at specific concentration were made in 16 steps. The labeled protein at a final concentration of 20 nM was equally mixed into each reaction. The final reaction mixtures were loaded into premium capillary chips (Monolith Cat# MO-AK002) and measured on a Monolith NT.115 instrument at 100% excitation power and 40% MST power at 25 $^\circ\text{C}$.

2. Results

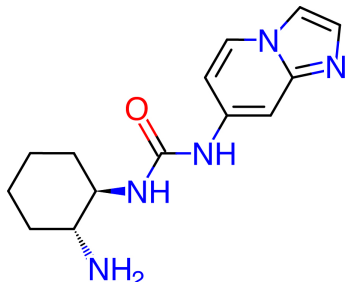
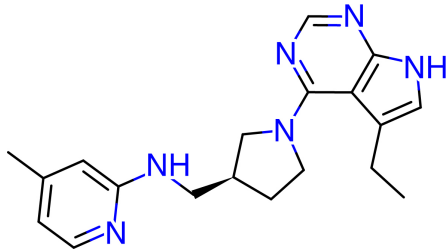
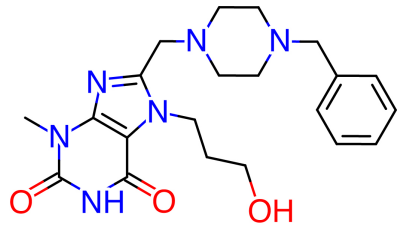
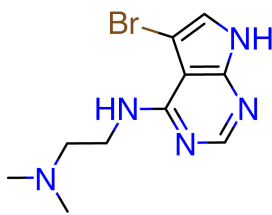
Virtual screening against nsp16 with docking into SAM-binding site of the enzyme was carried out. During in silico screening, a chemical space formed by three chemical libraries was selected: Enamine Coronavirus Library, Enamine Nucleoside Mimetics Library, and Chemdiv Nucleoside Analogue Library. After docking using SOL, 242 best scored compounds were selected for semiempirical quantum chemistry calculations to confirm or refute their affinity to nsp16. The selection criteria were described in [42]. Relying upon predicted values of the SOL score, binding enthalpies and binding modes, we selected 21 compounds for purchasing and further experimental testing. All 21 compounds were obtained, but 10 of them precipitated out of solution and their activity was not measured. For the remaining 11 compounds, dissociation constants were measured using Monolith NT.115. Structures of the measured 11 compounds and calculated values of the SOL scoring function and the binding enthalpy, as well as the measured dissociation constant K_d are given in Tab. 1.

Table 1. Best candidate inhibitors selected for experimental testing, their calculated SOL score, binding enthalpy ΔH_{bind} , and measured dissociation constant K_d

Compound	Structure	SOL score, kcal/mol	1-st cluster popul.	ΔH_{bind} , kcal/mol	K_d , μM
Z195979162		-5.24	40	-53.4	2.0

Compound	Structure	SOL score, kcal/mol	1-st cluster popul.	ΔH_{bind} , kcal/mol	K_d , μM
Z445470482		-5.54	15	-60.0	>20
Z1129470080		-6.04	36	-38.3	>20
Z1333277068		-5.24	47	-53.8	5.0
Z1538127913		-6.13	34	-40.7	>20
Z1715767396		-5.38	23	-53.0	>20
Z2045761676		-6.76	4	-30.8	>20

Development of Novel Nsp16 Inhibitors as Potential Anti-SARS-CoV-2 Agents

Compound	Structure	SOL score, kcal/mol	1-st cluster popul.	ΔH_{bind} , kcal/mol	K_d , μM
Z2396606359		-5.81	30	-54.5	>20
Z2968942047		-6.15	17	-55.4	>20
C692-0494		-5.27	10	-48.4	>20
FF01-2805		-5.03	37	-37.7	>20

To verify measured values of binding affinity of our 11 compounds with complex of nsp10/16, we performed the same MST measurements of SAM (native substrate of nsp10/16). Our MST measurements showed SAM binding affinity of 12 μM , which was consistent with reported values. We also measured activities of two published nsp16 inhibitors shown in Fig. 1: for compounds **4** and **6** the following values of K_d were obtained 123 μM and 1.4 μM , which are compatible with the published IC_{50} values, 51 μM and 3.4 μM , respectively.

The MD trajectories of inhibitors discovered in this study, Z195979162 ($K_d = 2.0 \mu\text{M}$) and Z1333277068 ($K_d = 5.0 \mu\text{M}$), are presented in Fig. 3 together with trajectories of a positive control – sinefungin ($\text{IC}_{50} = 0.86 \mu\text{M}$), and a negative control, C692-0494 ($K_d > 20 \mu\text{M}$).

In Fig. 3, we see a clear difference in the stability of the complex with sinefungin and with nsp16/nsp10 binders we found, compared to the inactive C692-0494 ligand which explicitly leaves the SAM-binding site of nsp16. The maximal values of RMSD for C692-0494, Z1333277068, Z1333277062, and sinefungin are 44.3, 6.13, 3.55, and 2.06 \AA , respectively. The mean values of RMSD calculated for the whole trajectory except for first 10 ns are of similar magnitude

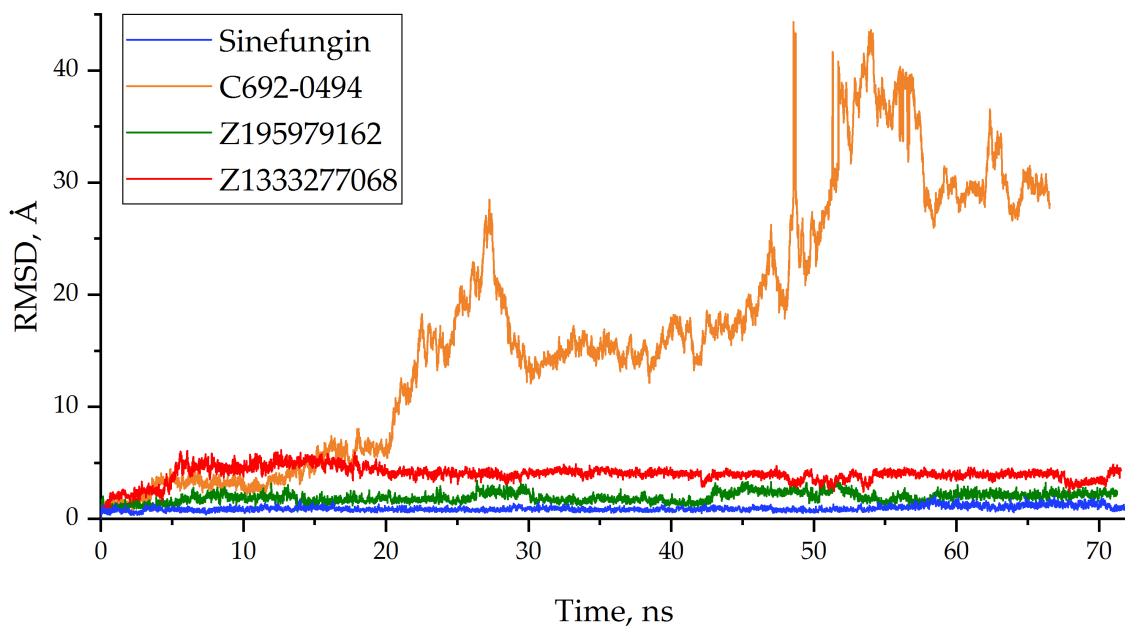


Figure 3. Stability of the nsp16 complex with each of four ligands along the MD trajectory. RMSD is the root-mean square deviation of the corresponding ligand from its docked position in the enzyme. Calculation of RMSD was performed only for heavy atoms of ligands

and equal 19.26, 4.07, 1.97, and 0.96 Å for C692-0494, Z1333277068, Z1333277062, and sinefungin, respectively. The latter shows a much stronger fixation near the docked position than the inhibitors Z1333277068 and Z1333277062. These values correspond to the observed relative 2'-O-MTase activity of these three inhibitors and the inactive ligand C692-0494. Notably, using two different water models, TIP3P and SPC, for C692-0494 resulted in similar molecular system behavior and a similar change in ligand RMSD along the trajectory.

Conclusion

COVID-19 continues to be associated with a significant health burden worldwide, and development of additional direct anti-SARS-CoV-2 treatments that act as alternatives to existing treatments is of great importance. Nsp16 protein provides important methylation reactions essential for the coronavirus life cycle and thereby represents a convenient target for which few actives are discovered to date. Using a computer-aided drug design approach, we managed to identify novel inhibitors of SARS-CoV-2 nsp16. To identify inhibitors, a virtual screening of three chemical libraries was performed using docking combined with semi-empirical quantum-chemical calculations of the enthalpy of binding of the ligand to the protein. The screened libraries contained 39350 unique 3D molecular structures. Relying upon predicted affinity values, we prioritized 11 compounds for *in vitro* testing. In MST assay, two inhibitors from Enamine Coronavirus Library, Z1333277062 and Z1333277068, were identified, which showed noticeable binding to nsp16/nsp10 complex with K_d values of 2.0 and 5.0 μM , respectively. The additional enzymatic assay might be applied in further steps to probe their inhibition profile. Compounds Z1333277062 and Z1333277068 belong to 1,4-disubstituted tetrahydropyridines and derivatives of pyrazole-5-carboxamide, respectively. In molecular dynamics studies, the complexes of these two inhibitors with nsp16 were stable for 70 ns of the simulated trajectory. Unlike existing

experimentally confirmed nsp16 inhibitors, the identified compounds do not possess structural patterns similar to the SAM co-substrate. Therefore, they may have a higher selectivity for off-target proteins than, for example, sinefungin. Thus, Z1333277062 and Z1333277068 can be good starting points for further hit expansion and optimization in the field of nsp16 inhibitors design.

Acknowledgments

The research is carried out using the equipment of the shared research facilities of HPC computing resources at Lomonosov Moscow State University, including the Lomonosov super-computer [49].

This research was financially supported by the Russian Foundation for Basic Research (RFBR, Russia), Project No. 20–51–55001 (A.S., D.K., I.I., A.T., and V.S. are grateful to the RFBR), and the National Natural Foundation of China (NSFC, China), Project No. 82161138005 (S.J. and Y.X. are grateful to the NSFC). All experimental works were carried out at the expense of Project No. 82161138005. Molecular modeling (construction of atomistic model of nsp10/nsp16 complex, docking, quantum chemistry, and MD calculations) were carried out at the expense of Project No. 20–51–55001.

This paper is distributed under the terms of the Creative Commons Attribution-Non Commercial 3.0 License which permits non-commercial use, reproduction and distribution of the work without further permission provided the original work is properly cited.

References

1. Chemdiv, nucleoside mimetics library, <https://www.chemdiv.com/catalog/focused-and-targeted-libraries/nucleoside-mimetics-library/>
2. Enamine, targeted libraries, <https://enamine.net/compound-libraries/targeted-libraries>
3. VMD: Visual Molecular Dynamics, <http://www.ks.uiuc.edu/Research/vmd/>
4. Stewart Computational Chemistry. MOPAC2016 (2016), <http://openmopac.net/MOPAC2016.html>
5. Schrodinger Release 2019-3: LigPrep (2019), <https://www.schrodinger.com/products/ligprep>
6. Baell, J.B., Holloway, G.A.: New Substructure Filters for Removal of Pan Assay Interference Compounds (PAINS) from Screening Libraries and for Their Exclusion in Bioassays. *Journal of Medicinal Chemistry* 53(7), 2719–2740 (2010). <https://doi.org/10.1021/jm901137j>
7. Berman, H.M., Westbrook, J., Feng, Z., *et al.*: The Protein Data Bank. *Nucleic Acids Research* 28(1), 235–242 (01 2000). <https://doi.org/10.1093/nar/28.1.235>
8. Bobieva, O., Bobrovs, R., Kaepe, I., *et al.*: Potent SARS-CoV-2 mRNA Cap Methyltransferase Inhibitors by Bioisosteric Replacement of Methionine in SAM Cosubstrate. *ACS Medicinal Chemistry Letters* 12(7), 1102–1107 (2021). <https://doi.org/10.1021/acsmchemlett.1c00140>

9. Bobrovs, R., Kanepe, I., Narvaiss, N., *et al.*: Discovery of SARS-CoV-2 Nsp14 and Nsp16 Methyltransferase Inhibitors by High-Throughput Virtual Screening. *Pharmaceuticals* 14(12) (2021). <https://doi.org/10.3390/ph14121243>
10. Chang, L.J., Chen, T.H.: NSP16 2'-O-MTase in Coronavirus Pathogenesis: Possible Prevention and Treatments Strategies. *Viruses* 13(4) (2021). <https://doi.org/10.3390/v13040538>
11. Citarella, A., Dimasi, A., Moi, D., *et al.*: Recent Advances in SARS-CoV-2 Main Protease Inhibitors: From Nirmatrelvir to Future Perspectives. *Biomolecules* 13(9) (2023). <https://doi.org/10.3390/biom13091339>
12. Decroly, E., Debarnot, C., Ferron, F., *et al.*: Crystal Structure and Functional Analysis of the SARS-Coronavirus RNA Cap 2'-O-Methyltransferase nsp10/nsp16 Complex. *PLOS Pathogens* 7(5), 1–14 (05 2011). <https://doi.org/10.1371/journal.ppat.1002059>
13. Decroly, E., Imbert, I., Coutard, B., *et al.*: Coronavirus Nonstructural Protein 16 Is a Cap-0 Binding Enzyme Possessing (Nucleoside-2'O)-Methyltransferase Activity. *Journal of Virology* 82(16), 8071–8084 (2008). <https://doi.org/10.1128/jvi.00407-08>
14. El Hassab, M.A., Ibrahim, T.M., Shoun, A.A., *et al.*: In silico identification of potential SARS COV-2 2'-O-methyltransferase inhibitor: fragment-based screening approach and MM-PBSA calculations. *RSC Advances* 11, 16026–16033 (2021). <https://doi.org/10.1039/D1RA01809D>
15. Feikin, D., Higdon, M., Abu-Raddad, L., *et al.*: Duration of effectiveness of vaccines against SARS-CoV-2 infection and COVID-19 disease: results of a systematic review and meta-regression. *The Lancet* 399(10328), 924–944 (02 2022). [https://doi.org/10.1016/S0140-6736\(22\)00152-0](https://doi.org/10.1016/S0140-6736(22)00152-0)
16. Ferron, F., Decroly, E., Selisko, B., Canard, B.: The viral RNA capping machinery as a target for antiviral drugs. *Antiviral Research* 96(1), 21–31 (2012). <https://doi.org/10.1016/j.antiviral.2012.07.007>
17. Gao, K., Wang, R., Chen, J., *et al.*: Methodology-Centered Review of Molecular Modeling, Simulation, and Prediction of SARS-CoV-2. *Chemical Reviews* 122(13), 11287–11368 (2022). <https://doi.org/10.1021/acs.chemrev.1c00965>
18. Gil, C., Ginex, T., Maestro, I., *et al.*: COVID-19: Drug Targets and Potential Treatments. *Journal of Medicinal Chemistry* 63(21), 12359–12386 (2020). <https://doi.org/10.1021/acs.jmedchem.0c00606>
19. Gomes, J.P.A., de Oliveira Rocha, L., Leal, C.E.Y., de Alencar Filho, E.B.: Virtual screening of molecular databases for potential inhibitors of the NSP16/NSP10 methyltransferase from SARS-CoV-2. *Journal of Molecular Structure* 1261, 132951 (2022). <https://doi.org/10.1016/j.molstruc.2022.132951>
20. Gowers, R., Linke, M., Barnoud, J., *et al.*: MDAnalysis: A Python package for the rapid analysis of molecular dynamics simulations. In: *SciPy*. pp. 98–105 (01 2016). <https://doi.org/10.25080/Majora-629e541a-00e>

21. Halgren, T.A.: MMFF VII. Characterization of MMFF94, MMFF94s, and other widely available force fields for conformational energies and for intermolecular-interaction energies and geometries. *Journal of Computational Chemistry* 20(7), 730–748 (1999). [https://doi.org/10.1002/\(SICI\)1096-987X\(199905\)20:7<730::AID-JCC8>3.0.CO;2-T](https://doi.org/10.1002/(SICI)1096-987X(199905)20:7<730::AID-JCC8>3.0.CO;2-T)
22. Hunter, J.: Matplotlib: A 2D Graphics Environment. *Computing in Science & Engineering* 9, 90–95 (06 2007). <https://doi.org/10.1109/MCSE.2007.55>
23. Klamt, A., Schuurmann, G.: COSMO: a new approach to dielectric screening in solvents with explicit expressions for the screening energy and its gradient. *Journal of the Chemical Society, Perkin Transactions 2* pp. 799–805 (1993). <https://doi.org/10.1039/P29930000799>
24. Klima, M., Khalili Yazdi, A., Li, F., *et al.*: Crystal structure of SARS-CoV-2 nsp10nsp16 in complex with small molecule inhibitors, SS148 and WZ16. *Protein Science* 31(9), e4395 (2022). <https://doi.org/10.1002/pro.4395>
25. Krafcikova, P., Silhan, J., Nencka, R., Boura, E.: Structural analysis of the SARS-CoV-2 methyltransferase complex involved in RNA cap creation bound to sinefungin. *Nature Communications* 11(1), 3717 (07 2020). <https://doi.org/10.1038/s41467-020-17495-9>
26. Kutov, D.C., Katkova, E.V., Sulimov, A.V., *et al.*: Influence of the method of hydrogen atoms incorporation into the target protein on the protein-ligand binding energy. *Bulletin of the South Ural State University. Series “Mathematical Modelling, Programming and Computer Software”* 10(3), 94–107 (2017). <https://doi.org/10.14529/mmp170308>
27. Lin, S., Chen, H., Ye, F., *et al.*: Crystal structure of SARS-CoV-2 nsp10/nsp16 2'-O-methylase and its implication on antiviral drug design. *Signal Transduction and Targeted Therapy* 5(1), 131 (12 2020). <https://doi.org/10.1038/s41392-020-00241-4>
28. Lipsitch, M., Krammer, F., Regev-Yochay, G., *et al.*: SARS-CoV-2 breakthrough infections in vaccinated individuals: measurement, causes and impact. *Nature Reviews Immunology* 22(1), 57–65 (12 2021). <https://doi.org/10.1038/s41577-021-00662-4>
29. Malone, B., Urakova, N., Snijder, E., Campbell, E.: Structures and functions of coronavirus replication/transcription complexes and their relevance for SARS-CoV-2 drug design. *Nature Reviews Molecular Cell Biology* 23(1), 21–39 (11 2021). <https://doi.org/10.1038/s41580-021-00432-z>
30. Mohammad, A., Alshawaf, E., Marafie, S.K., *et al.*: Molecular Simulation-Based Investigation of Highly Potent Natural Products to Abrogate Formation of the nsp10nsp16 Complex of SARS-CoV-2. *Biomolecules* 11(4), 573 (2021). <https://doi.org/10.3390/biom11040573>
31. Nguyen, H.L., Thai, N.Q., Li, M.S.: Identifying inhibitors of NSP16-NSP10 of SARS-CoV-2 from large databases. *Journal of Biomolecular Structure and Dynamics* 41(15), 7045–7054 (2023). <https://doi.org/10.1080/07391102.2022.2114941>
32. Owen, D.R., Allerton, C.M.N., Anderson, A.S., *et al.*: An oral SARS-CoV-2 Mpro inhibitor clinical candidate for the treatment of COVID-19. *Science* 374(6575), 1586–1593 (2021). <https://doi.org/10.1126/science.abl4784>

33. Phillips, J.C., Hardy, D.J., Maia, J.D.C., *et al.*: Scalable molecular dynamics on CPU and GPU architectures with NAMD. *The Journal of Chemical Physics* 153(4), 044130 (2020). <https://doi.org/10.1063/5.0014475>
34. Ramanathan, A., Robb, G.B., Chan, S.H.: mRNA capping: biological functions and applications. *Nucleic Acids Research* 44(16), 7511–7526 (06 2016). <https://doi.org/10.1093/nar/gkw551>
35. Romano, M., Ruggiero, A., Squeglia, F., *et al.*: A Structural View of SARS-CoV-2 RNA Replication Machinery: RNA Synthesis, Proofreading and Final Capping. *Cells* 9(5), 1267 (2020). <https://doi.org/10.3390/cells9051267>
36. Romanov, A.N., Jabin, S.N., Martynov, Y.B., *et al.*: Surface Generalized Born method: a simple, fast and precise implicit solvent model beyond the Coulomb approximation. *The Journal of Physical Chemistry A: Molecules, Clusters, and Aerosols* 108(43), 9323–9327 (2004). <https://doi.org/10.1021/jp046721s>
37. Rosas-Lemus, M., Minasov, G., Shuvalova, L., *et al.*: High-resolution structures of the SARS-CoV-2 2'-O-methyltransferase reveal strategies for structure-based inhibitor design. *Science Signaling* 13(651), eabe1202 (2020). <https://doi.org/10.1126/scisignal.abe1202>
38. Shi, L., Wen, Z., Song, Y., *et al.*: Computational investigation of potent inhibitors against SARS-CoV-2 2'-O-methyltransferase (nsp16): Structure-based pharmacophore modeling, molecular docking, molecular dynamics simulations and binding free energy calculations. *Journal of Molecular Graphics and Modelling* 117, 108306 (2022). <https://doi.org/10.1016/j.jmgm.2022.108306>
39. Silva, L.R., da Silva Santos-Junior, P.F., de Andrade Brandao, J., *et al.*: Druggable targets from coronaviruses for designing new antiviral drugs. *Bioorganic & Medicinal Chemistry* 28(22), 115745 (2020). <https://doi.org/10.1016/j.bmc.2020.115745>
40. Stewart, J.: Optimization of parameters for semiempirical methods VI: More modifications to the NDDO approximations and re-optimization of parameters. *Journal of molecular modeling* 19(1), 1–32 (1 2013). <https://doi.org/10.1007/s00894-012-1667-x>
41. Stewart, J.J.: Application of localized molecular orbitals to the solution of semiempirical self-consistent field equations. *International Journal of Quantum Chemistry* 58(2), 133–146 (1996). [https://doi.org/10.1002/\(SICI\)1097-461X\(1996\)58:2%3C133::AID-QUA2%3E3.0.CO;2-Z](https://doi.org/10.1002/(SICI)1097-461X(1996)58:2%3C133::AID-QUA2%3E3.0.CO;2-Z)
42. Sulimov, A., Kutov, D., Ilin, I., *et al.*: Novel Inhibitors of 2'-O-Methyltransferase of the SARS-CoV-2 Coronavirus. *Molecules* 27(9), 2721 (2022). <https://doi.org/10.3390/molecules27092721>
43. Sulimov, A.V., Kutov, D.C., Oferkin, I.V., *et al.*: Application of the Docking Program SOL for CSAR Benchmark. *Journal of Chemical Information and Modeling* 53(8), 1946–1956 (2013). <https://doi.org/10.1021/ci400094h>

44. Sulimov, V.B., Ilin, I.S., Kutov, D.C., Sulimov, A.V.: Development of docking programs for Lomonosov supercomputer. *Journal of the Turkish Chemical Society Section A: Chemistry* 7(1), 259–276 (Feb 2020). <https://doi.org/10.18596/jotcsa.634130>
45. Tazikeh-Lemeski, E., Moradi, S., Raoufi, R., *et al.*: Targeting SARS-COV-2 non-structural protein 16: a virtual drug repurposing study. *Journal of Biomolecular Structure and Dynamics* 39(13), 4633–4646 (2021). <https://doi.org/10.1080/07391102.2020.1779133>
46. Tiwari, V., Beer, J.C., Sankaranarayanan, N.V., *et al.*: Discovering small-molecule therapeutics against SARS-CoV-2. *Drug Discovery Today* 25(8), 1535–1544 (2020). <https://doi.org/10.1016/j.drudis.2020.06.017>
47. Vanommeslaeghe, K., Hatcher, E., Acharya, C., *et al.*: CHARMM general force field: A force field for drug-like molecules compatible with the CHARMM all-atom additive biological force fields. *Journal of Computational Chemistry* 31(4), 671–690 (2010). <https://doi.org/10.1002/jcc.21367>
48. Viswanathan, T., Arya, S., Chan, S.H., *et al.*: Structural basis of RNA cap modification by SARS-CoV-2. *Nature Communications* 11(1), 3718 (07 2020). <https://doi.org/10.1038/s41467-020-17496-8>
49. Voevodin, V.V., Antonov, A.S., Nikitenko, D.A., *et al.*: Supercomputer lomonosov-2: Large scale, deep monitoring and fine analytics for the user community. *Supercomputing Frontiers and Innovations* 6(2), 4–11 (Jun 2019). <https://doi.org/10.14529/jsfi190201>
50. Walls, A.C., Park, Y.J., Tortorici, M.A., *et al.*: Structure, Function, and Antigenicity of the SARS-CoV-2 Spike Glycoprotein. *Cell* 181(2), 1735 (2020). <https://doi.org/10.1016/j.cell.2020.02.058>
51. Wrapp, D., Wang, N., Corbett, K., *et al.*: Cryo-EM structure of the 2019-nCoV spike in the prefusion conformation. *Science* 367(6483), 1260–1263 (02 2020). <https://doi.org/10.1126/science.abb2507>
52. Wu, C., Liu, Y., Yang, Y., *et al.*: Analysis of therapeutic targets for SARS-CoV-2 and discovery of potential drugs by computational methods. *Acta Pharmaceutica Sinica B* 10(5), 766–788 (2020). <https://doi.org/10.1016/j.apsb.2020.02.008>
53. Wu, Y., Li, Z., Zhao, Y.S., *et al.*: Therapeutic targets and potential agents for the treatment of COVID-19. *Medicinal Research Reviews* 41(3), 1775–1797 (2021). <https://doi.org/10.1002/med.21776>